Sub-femtogram simultaneous elemental detection in multicomponent nanomatrices using laser-induced plasma emission spectroscopy within atmospheric pressure optical traps

Pablo Purohit, Francisco J. Fortes and J. Javier Laserna*

UMALASERLAB, Departamento de Química Analítica, Universidad de Málaga, C/Jiménez Fraud 4, Malaga 29010, Spain. Corresponding author's email: laserna@uma.es

ABSTRACT: Simultaneous detection of multiple constituents in the characterization of state-of-the-art nanomaterials is an elusive topic to a majority of the analytical techniques covering the field of nanotechnology. Optical catapulting (OC) and optical trapping (OT) have recently been combined with laser-induced breakdown spectroscopy (LIBS) to provide single nanoparticle resolution and attogram detection power. In the present work, the multielemental capabilities of this approach are demonstrated by subjecting two different types of nanometric ferrite particles to LIBS analysis. Up to three metallic elements in attogram quantities are consistently detected within single laser events. Individual excitation efficiency for each species is quantified from particle spectra showing an exponential correlation between photon production and the energy of the upper level of the monitored atomic line. Moreover, a new sampling strategy based in skimmer-like 3D printed cones which allows for thin dry nanoparticle aerosols to be formed via optical catapulting is introduced. Enhanced sampling resulted in an increase of the sampling throughput by facilitating stable atmospheric-pressure optical trapping of individual particles and spectroscopic chemical characterization within a short time frame

Introduction

The interest in accurate characterization of every component present in cutting-edge nanomaterials is increasing proportionally to their design complexity.[1-4] Functional elements that might be present within engineered or natural occurring nanoparticles (NPs) range from light atoms to metalloids like Si, heavier noble metals such as Ag or Au[5] or metallic oxides. The latter NPs are of interest in nanostructure research for a variety of application, e.g. as support for further functionalized materials[6-7] and as catalyst themselves.[8-11] The numerous singularities of nanosamples represent a challenge in constant evolution to the Analytical Chemistry community.

Routine analytical techniques in laboratories such as ICP-AES,[12-13] GF-AAS,[14-15] IR spectroscopy[16] or conventional ICP-MS[17] can provide complete depictions of samples containing populations of nanotargets, yet, with the exception of MS, do not operate at single particle (SP) level, are limited in the number detectable species, unsuitable for organics or difficult to use for certain inorganics. Single nanoparticle analysis has for many years struggled to establish itself as a necessary application in studies other than research such as quality control, yet with designs relying heavily on tight control over parameters including shape and composition, the occlusion of non-desired chemical species in individual particles can be crucial for perfect function of materials, hence justifying the efforts in SP analysis. Although numerous approaches to SP-MS have been reported,[18-20] this technique is not able to provide panoramic chemical information within the frame of a single reading and often involves tedious data treatment procedures.

Laser-induced breakdown spectroscopy (LIBS) is commonly regarded as a versatile technique able to adapt to multiple extreme scenarios[21-22] and has been recognized as an excellent method for aerosol science since early stages of its development.[23-24] Aerosol-related LIBS studies were the precursor to SP-LIBS analysis which was successfully applied to microparticles isolated in an electrodynamic balance by Järvinen and coworkers.[25-26] Recently, a novel approach named OC-OT-LIBS was introduced as a promising method for analysis of single NPs.[27] Under this methodology, particles are stably trapped in air at atmospheric pressure and can be conveniently manipulated for precise positioning prior to LIBS analysis. As a result, the emission spectra from the individually trapped particles is acquired. Thus, the integration of optical catapulting (OC), optical trapping (OT) and LIBS acting sequentially permit straightforward identification of the material inspected. This platform has been successfully used for the chemical analysis of single micro- and nanoparticles down to 25 nm in diameter for Cu NPs[28-29] leading to direct detection of masses in the attogram regime and yielding Limits of Detection (LODs) unprecedented in optical emission spectroscopy such as 58.9±1.8 ag for Cu NPs.

Among capabilities still to be addressed using OC-OT-LIBS are its sampling throughput as well as its relation to other techniques and the simultaneous detection of multiple analytes within a single NP inherent to LIBS. In this work, an enhanced sampling strategy is tested seeking to drastically reduce the analysis duration by limiting the number of particles reaching the optical trap and remaining in suspension in the sample chamber during LIBS probing. Multielemental analysis was performed using binary and tertiary spinel samples, $CuFe_2O_4$ and $CuZn_{1-x}Fe_2O_4$, respectively. Herein, simultaneous detection of multiple metallic species all present in attogram quantities in nanomatrices of masses in the low femtogram range is demonstrated. Individual limits of detection are provided for each species along individual excitation efficiency, which fundaments the recorded data and provides insight on the laser-induced mechanisms causing the dissociation and excitation of trapped NPs.

Experimental section

Samples

Inverse spinels $CuFe_2O_4$ and $CuZn_{1-x}Fe_2O_4$ nanoparticles of 90±18 nm diameter (MKNano, Canada) were subjected to LIBS characterization. Physical and compositional properties for both samples are provided in **Table 1**. Chemical formula of the Zn-containing ferrites was assumed to be $CuZnFe_2O_4$ to simplify the mass calculation due to its non-stoichiometric nature and to account for particle-to-particle Zn fraction changes, which was weighed during data averaging process. Provided density values are those of the bulk materials.

Sample preparation

Dry nanopowders were used throughout the experiments. Samples consisted of qualitative portions of particles (normally, few micrograms) placed on a 200 µm thick microscope cover glass serving as platform. To prevent sample losses caused by diffusion into open air upon laser-induced shockwave impacts, a 10 mm light path disposable plastic cuvette was glued to each cover glass, conforming the sample chamber.

Instrumental setup

Instrument configuration is thoroughly described in references **27** and **28**. Briefly, a ns-pulsed laser emitting at 1064 nm and focused through a 20x long working distance microscope objective was used to eject the nanopowders into aerosol form by creating a shockwave that propagated through the sample platform. Perpendicular to the catapulting laser, and focused by the same objective, impinged a CW laser centered at 532 nm. This laser constituted the optical trap at approximately 15 mm from the chamber base. Location of the trap as well as the position of trapped particles was adjusted by manipulating the microscope objective along the z axis. The whole system was aligned to a (0, 0, 0) coordinate dictated by the intersection of the sampling laser and the particle under inspection as registered using an iCCD camera **27**. Once the particle was conveniently placed and the aerosol flow ceased, LIBS analysis was performed using a 10x microscope objective to focus a 6 ns, 1064 nm laser pulse on the particle. The energy density was kept constant at 3.3 x 10^3 J cm^{-2} thus sparking an air plasma that engulfed the trapped NP. Plasma light was directed by a pair of 2" bi-convex lenses into the tip of a 600 µm core diameter optical fiber, connected to a time-integrated spectrometer. Synchronization of the lasers was externally controlled by a pair of pulse and delay generator which allowed the control of the interpulse delay and data acquisition parameters. Acquisition delay time for LIBS analysis was kept at 5.28 µs, thus minimizing spectral background. **Figure 1A** summarizes the essential components of the OC-OT-LIBS system.

Table 1. Physical properties of the samples and mass fraction for each element in both types of NPs.

	$CuFe_2O_4$	$CuZnFe_2O_4$
Particle size (nm)	90±18	90±18
Density (g cm^{-3})	5.4	5.5
Average particle mass (fg)	2.06	2.09
Molecular weight (g $mole^{-1}$)	239.23	304.62

$CuFe_2O_4$	w%	Mass fraction (fg)
Cu	26.56	0.55
Fe	46.68	0.96
O	26.75	0.55

$CuZnFe_2O_4$	w%	Mass fraction (fg)
Cu	20.85	0.43
Zn	21.46	0.45
Fe	36.66	0.77
O	21.01	0.44

Enhanced sampling strategy

In previous articles, a limiting factor to the OC-OT-LIBS technology was the sampling throughput. High density of catapulted aerosols along with elongated persistence times of the suspended particles, which iteratively recirculate inside the sampling chamber due to naturally-occurring convection currents, contributed to extend the length of sampling periods. As a consequence, the aforementioned convection currents increase the number of collisions, resulting in occasional expulsion of trapped particles from the trapping volume. With the objective of thinning aerosol streams and improving the sampling throughput, 3D-printed resin cones, emulating skimmer cones used in mass spectrometry, were tested. The dimensions of the *sampling cones* are depicted in **Figure 1B**. Cones were designed to precisely adjust to the chamber width and allowed an easy alignment of the trapping laser beam while keeping intact the location of the optical trap. Tip aperture diameter was 2 mm to accommodate the size of the beam waist while far from the focus. As shown in **Figure 1C**, by introducing a sampling cone in the chamber, the aerosol stream reaching the optical trap was restricted to that propagating collinear to the cone aperture and the laser trapping. Presence of recirculating material, propelled in every direction during the OC stage, was considerably reduced as it impacted the inner walls of the cone. To evaluate the differences between both strategies, *with* and *without sampling cones*, the aerosol streams were monitored by an iCCD camera.

Data processing and identification of single particle events

Spectral range covered by the detector covered wavelengths between 260 and 430 nm where the three elements under study feature strong emission lines which are not interfered by emissions from the air plasma. The most intense emission lines featured in recorded spectra were used for further studies, i.e. Fe (II) at λ = 274.69 nm, Cu (I) at λ = 324.75 nm and Zn (I) at λ = 334.50 nm. The ionic Fe line was chosen on the basis of its consistent particle-to-particle detectability and improved SNR when compared to Fe (I) emission at 302.04 nm. In bulk studies, the Cu (I) line at 324.75 nm has a tendency to self-absorption which was not observed in SP spectra, this could indicate low number density of Cu atoms in the ground state populating the collected plasma portion[30] and, subsequently high excitation efficiency. To extract the net intensity of the emission, background values were calculated for each emission line by averaging 4 nm of their closest signal-free region. Cu (I) signal was used to verify whether recorded spectra corresponded to a single NP or a particle cluster. The system was calibrated by using Cu NPs of 25, 50 and 70 nm in average diameter.

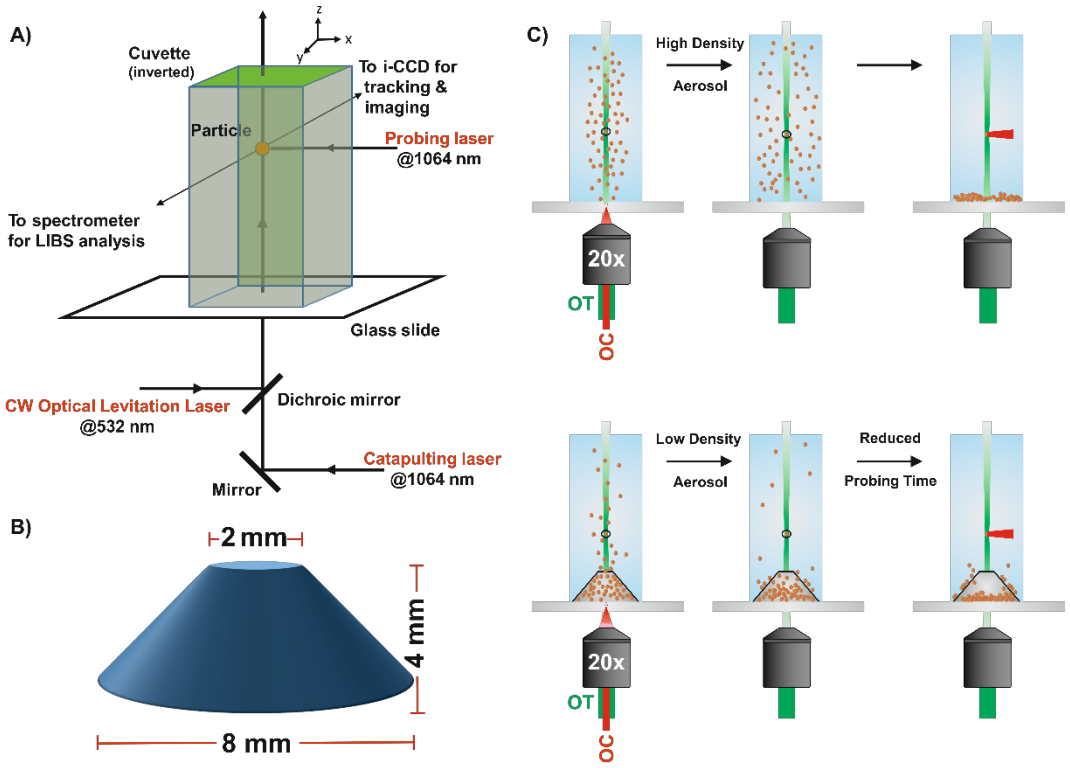

Figure 1. A) Simplified experimental setup featuring the main laser-based lines described in the main text. A visualization line consisting in a biconvex lens and an iCCD camara was located collinear to the LIBS detection. B) 3D printed cones used for the enhanced sampling strategy. C) Illustration of both sampling schemes tested herein. Concept of the enhanced route is depicted in the bottom row.

Figure 2 features average net intensity of the line Cu (I) at 324.75 nm for ten single-particle events plotted as function of the particle mass. A high correlation between both parameters was observed. Since the mass fraction of Cu in both ferrites was known, net LIBS signals for Cu resulting from single $CuFe_2O_4$ and $CuZnFe_2O_4$ NPs analysis were expected to fit properly in the calibration equation. This was motivated by previous results which demonstrated that particles below 2 µm fully dissociate in our system yielding signals proportional to the analyte mass occluded in the laser-induced plasma [27- 29]. Therefore, good adaptation of the processed signals to the linear fit was used as the condition to evidence whether the number of probed particles was one or above one.

Signals meeting the criteria of signal-to-noise ratio (SNR) >3 were considered to be within the limit of detection of OC-OT-LIBS. Limit of detection (LOD) for Fe and Zn were calculated as:

$$LOD = \frac{3\ C\ RSD_B}{SBR}$$

Where C is the concentration in w/w %, RSD_B is the relative standard deviation of the blank and SBR is the net signal to background ratio. LOD for Cu was estimated from the linear regression in **Figure 2**. To avoid misestimating background-related quantities, air plasmas ignited in sample-free cuvettes were used as blanks. In this way, alterations originating from seeding effects due to aerosolized NPs close to the focal region are obviated.

Results and discussion

Sampling Statistics

Following the scheme proposed in **Figure 1C**, a number of twenty laser events were acquired under each sampling strategy. OC-OT-LIBS analysis were performed using $CuFe_2O_4$ NPs of 90 nm in diameter. Differences among both sampling schemes were appreciable, and the results are summarized in **Table 2**. In our study, the *trapping efficiency* was defined as the number of catapulting events resulting in a particle entering the optical trap and remaining occluded for a period of time long enough to proceed with LIBS characterization. Trapping was considered stable once no confined particle-aerosol collisions could be observed in the iCCD camera. In this aspect, the *average time for stable trapping* was reduced by ca. 50% when using the sampling cones. Thus, the trapped particles would remain steady performing ordinary Brownian motion after 1.5-2.2 min from the aerosol onset.

Table 2. Sampling statistics for n = 20 under both described sampling schemes.

	Regular sampling scheme	Enhanced sampling scheme
Trapping efficiency (%)	76%	93%
Average time for stable trapping (min)	~ 4.0	< 2.0
Average time for complete analysis (min)	6.8	3.2
SP events (%)	31%	56%
Sampling throughput (NP $hour^{-1}$)	~ 9	~ 20

Studies were completed once aerosol stream relaxed and no longer interfered with the focal region of the laser employed for LIBS analysis. Hence, the *average time for complete analysis* was also shortened in time by a factor of 2.13. Improvements in sampling statistics were related to the significant amount of particles remaining within the cone walls after the catapulting event. With the objective of evaluating whether acquired emission signals originated from individual particles or a clusters, the Cu (I) emission at 324.75 nm of each recorded spectra was fitted into the linear regression shown in **Figure 2**, perfectly associating each laser event to a defined particle mass. As a result, the *percentage of SP events* was higher when using the sampling cones, greater than 50%, and the *total sampling throughput* was improved by a factor of 2. This experiment also proved that sampling cones prevented from aggregates reaching the optical trap and the formation of clusters and agglomerates in the focus.

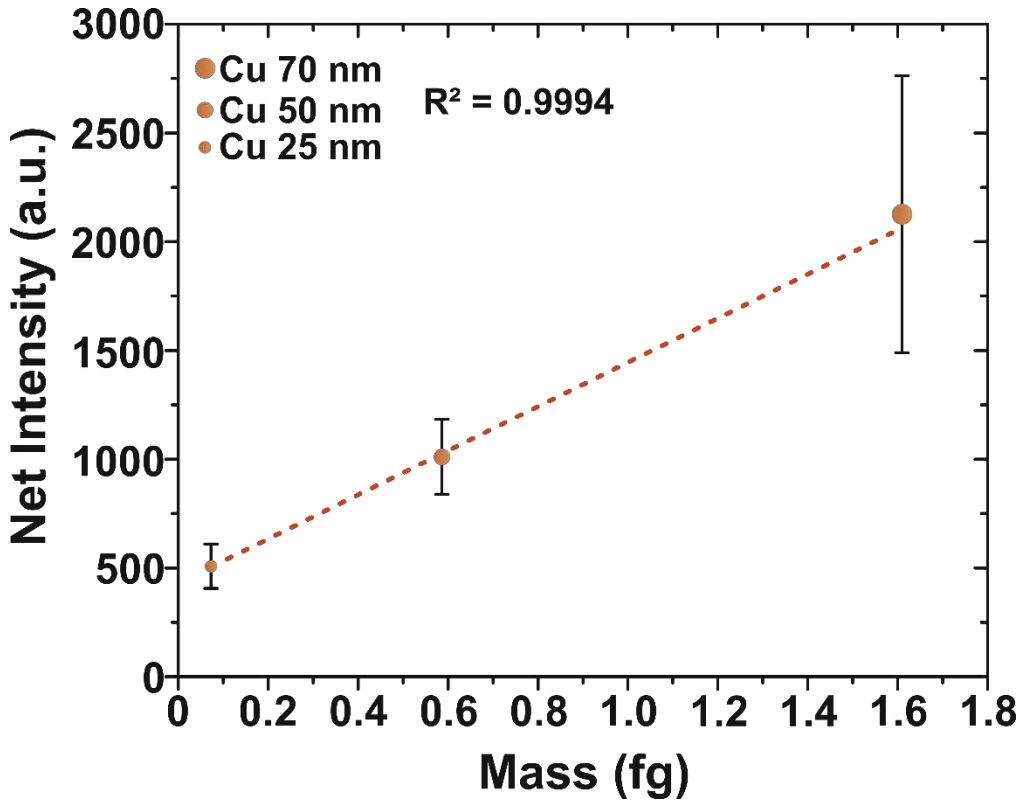

Figure 2. Cu signal calibration of the OC-OT-LIBS platform using three different average particle sizes. In agreement with previous results on this subject, response was directly proportional to ablated mass, thus verifying that only single particles were probed in each case. Moreover, the limit of quantification (LOQ) of the approach was calculated as LOQ = yb +10sb =236 ag, hence confirming that Cu quantification in the ferrites was reliable under our experimental conditions.

Figure 3 presents the evolution of aerosol streams as a function of time under each sampling strategy. As observed in the images, the use of a sampling cone favored the formation of a substantially thinner aerosol stream. The frames captured at 105 s revealed that, in contrast, the regular sampling scheme featured heavy aerosol flow. It is worth highlighting that at 105 s barely any suspended material other than the stably trapped particle could be observed when using the sampling cone. Finally, once the trapped particle was stabilized, it could be conveniently manipulated and positioned at the (0,0,0) coordinate for LIBS analysis as shown in **Figure 3I-J**. Thereby, the inclusion of sampling cones enhances the efficiency of the technology to fully characterize NP populations by resulting in a twofold increment of the number of readings per hour and more favorable probing conditions.

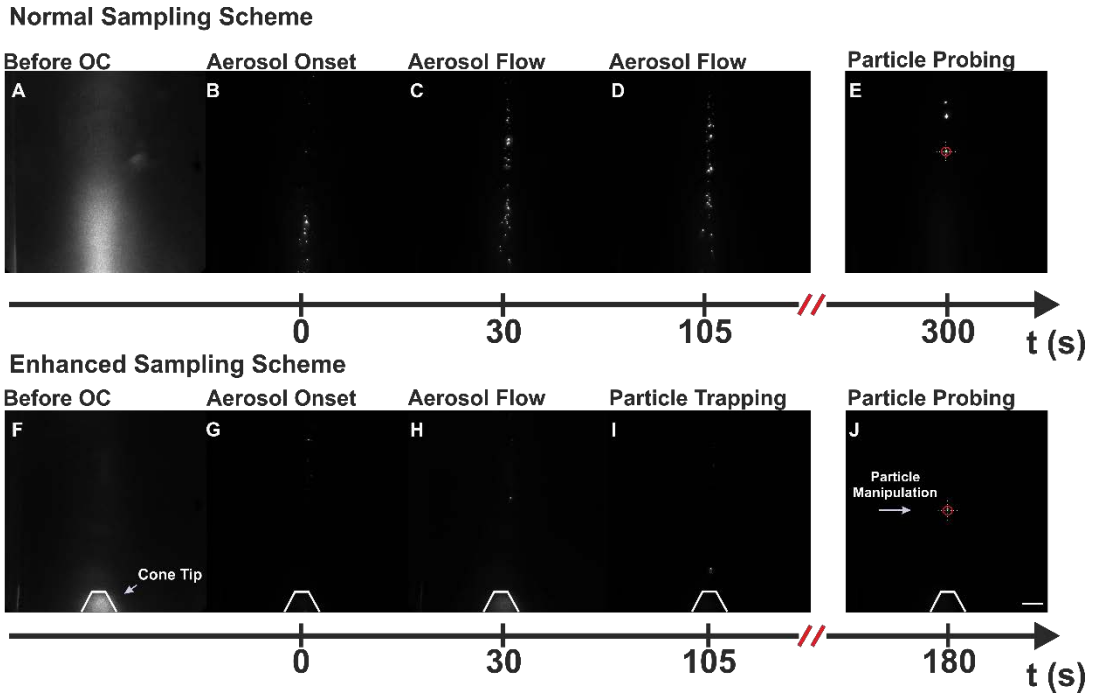

Figure 3. iCCD images for an analysis performed under A-E) regular sampling scheme and F-J) improved sampling scheme. Frames were recorded at identical times up to stable particle trapping, which happens at t = 105 s for the improved scheme, where axis breaks to the moment before LIBS probing. For reference, the illuminated cone tip is shown in bottom row images. Scale bar is 300 µm.

Multilelemental detection

All the metallic atoms constituting both ferrites were successfully detected by LIBS. Average spectra of 29 single particle events for $CuFe_2O_4$ and 17 events for $CuZnFe_2O_4$ are shown in **Figure 4**. Average net Intensity of Cu (I) at 324.75 nm was calculated as 919.4±193.1 a.u. for $CuFe_2O_4$ and 811.7±137.9 a.u. for $CuZnFe_2O_4$. When interpolated in the calibration curve, regression analysis resulted in r = 0.995, indicating a high agreement degree between the calculated Cu mass for each oxide and the experimental mass. Signal-to-noise ratios were 14 for $CuFe_2O_4$ and 20 for $CuZnFe_2O_4$. Emission intensity for the ionic line Fe (II) at 274.91 nm was slightly higher for $CuZnFe_2O_4$: Net I ($CuFe_2O_4$) = 247.3 ± 74.1 (SNR = 7), Net I ($CuZnFe_2O_4$) = 320.5 ± 124.0 (SNR = 6). This fact may seem counterintuitive provided the ca. 20% lower Fe content available in this ferrite. In previous works, single particles were found to undergo dissociation and excitation in agreement with the mechanisms proposed by Hohreiter and Hahn.[31] Briefly, the surrounding air plasma forming alongside the particle plasma, transfers energy to the particle in the form of heat which promotes the breaking of the particle chemical bonds thus freeing atoms into the plasma. Free atoms are then excited to emissive levels also by the air plasma. Both transferences are rate limited. Zn^{+2} partially substitutes Cu^{+2} in $CuZnFe_2O_4$, introducing a weaker, and subsequently, easier to dissociate bond in the crystalline lattice ($\Delta H_f°_{Cu\text{-}O}$ = 343 Kcal mol^{-1} whereas $\Delta H_f°_{Zn\text{-}O}$ = 284 Kcal mol^{-1}). As the quantity of energy required by each particle to fully dissociate is smaller in the case of the Zn-containing ferrite, it is reasonable to assume that a larger fraction of the energy is available for excitation of the free atoms. Zn (I) at 334.50 exhibited a weak intensity profile (Net I = 60 ± 7.5 a.u.), barely within detectability (SNR = 3). Further details on this emission are provided in the section below. Individual LIBS spectra indicate that OC-OT-LIBS can directly and simultaneously detect masses as low as 770 ag of Fe and 450 ag of Zn with theoretical absolute LODs calculated from average spectra of 575 ag for Fe and 304 ag for Zn in multielemental matrices. Furthermore, the LOD for Cu (from the linear regression) was 37 ag. The use of sampling cones herein improved the LOD for Cu using the 324.75 nm line previously established at 58.9 ag[29] by ca. 37%.

Photon yield as a measure of excitation efficiency

For a better understanding of the phenomena occurring during the air plasma-particle interaction and the pathways followed during the atomization and the excitation of the samples, the photon budget was calculated as described elsewhere.[27-29] Quantification of photons emitted at a given wavelength provided a solid ground for interpretation of spectra and justification of the analytical performance of OC-OT-LIBS for each species. **Figure 5A** shows the absolute emission of photons per sample mass unit of

the lines used for LODs calculation along neighboring Fe signal to Fe (II) at 274.91 nm. Despite differences in the Cu $_{(324.75)}$/Cu $_{(327.39)}$ photon yield ratio found from one matrix to another, the total number of photons emitted by Cu atoms remained virtually constant.

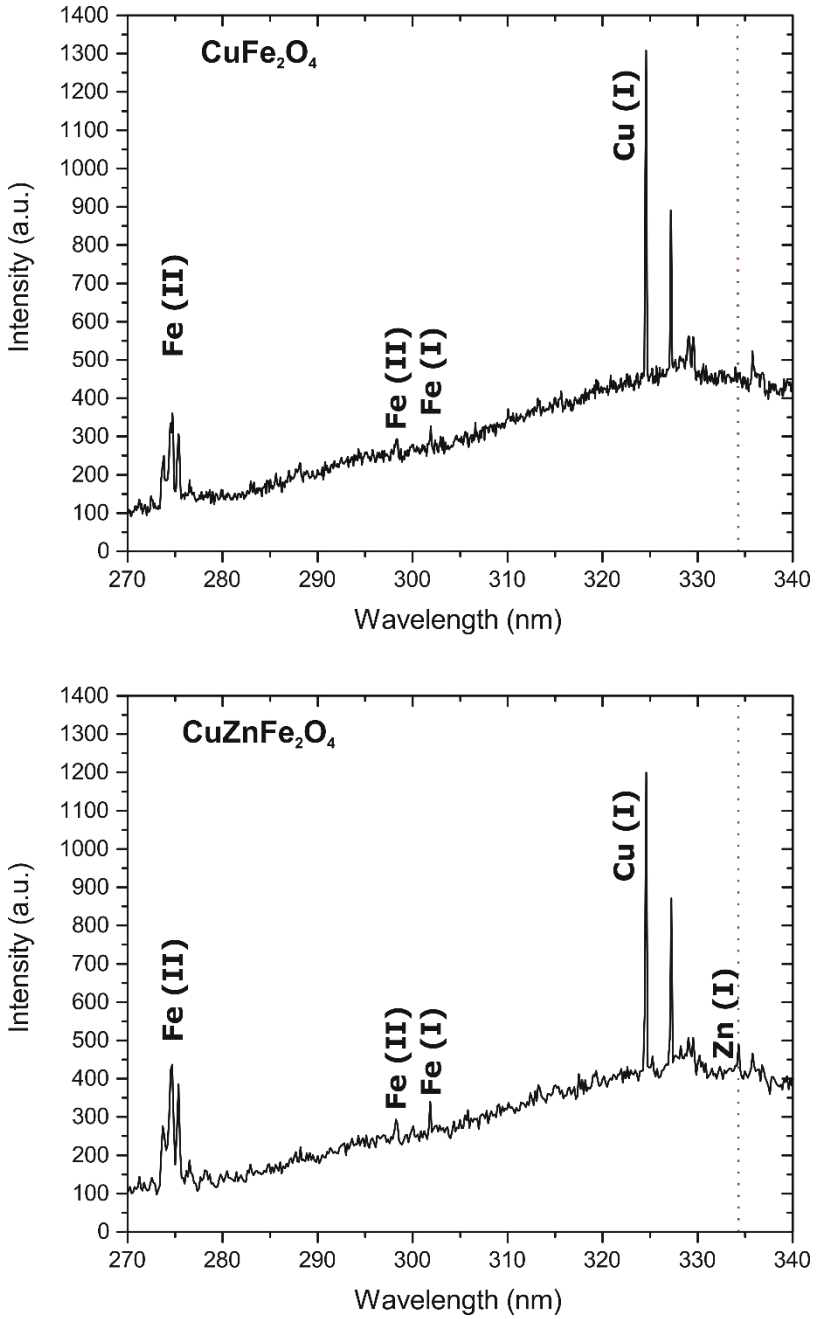

Figure 4. Average spectra of A) 29 single $CuFe_2O_4$ events and B) 17 single $CuZnFe_2O_4$ events. For better comparison, Zn line is marked with a discontinuous red line. Fe lines at 298.31 nm and 301.90 nm were not considered for statistics due to their lower intensity with respect to that of Fe (II) at 275.91 nm.

An average of 12.7 x 10^{21} photons g^{-1} were recorded from $CuFe_2O_4$ analysis while 12.5 x 10^{21} photons g^{-1} originated from $CuZnFe_2O_4$ NPs, indicating that both samples underwent plasma-particle interactions of similar efficiencies. Moreover, this fact pointed towards a potential saturation of the excitation process for similar-sized NPs with the whole atomic population of a certain element being promoted to emissive states by the air plasma. In agreement with spectral data, Fe atoms are more efficiently excited in $CuZnFe_2O_4$ as evidenced by the general increase in photon yield for every monitored line. Yield of the Zn transition was, as expected from LIBS results, poor featuring an order of magnitude less efficiency than other studied lines (5.41 x 10^{20}). Parameters affecting the intensity of an emission line include oscillator strength, transition probability and energy of the level to which electrons are promoted by the excitation source. **Figure 5B** shows the energy of the upper levels (E_1) as found in literature for lines considered in **Figure 4A** in addition to the gap (ΔE) separating E_1 and the ground level (E_0). E_1 for Zn emission at 334.50 nm was the highest of the seven considered transitions with E_1= 7.76 eV. In **Figure 5C**, the photon yield of each transit of $CuZnFe_2O_4$ is plotted as function of E_1. A decaying profile with acceptable correlation coefficient was found upon data fitting to an exponential function.

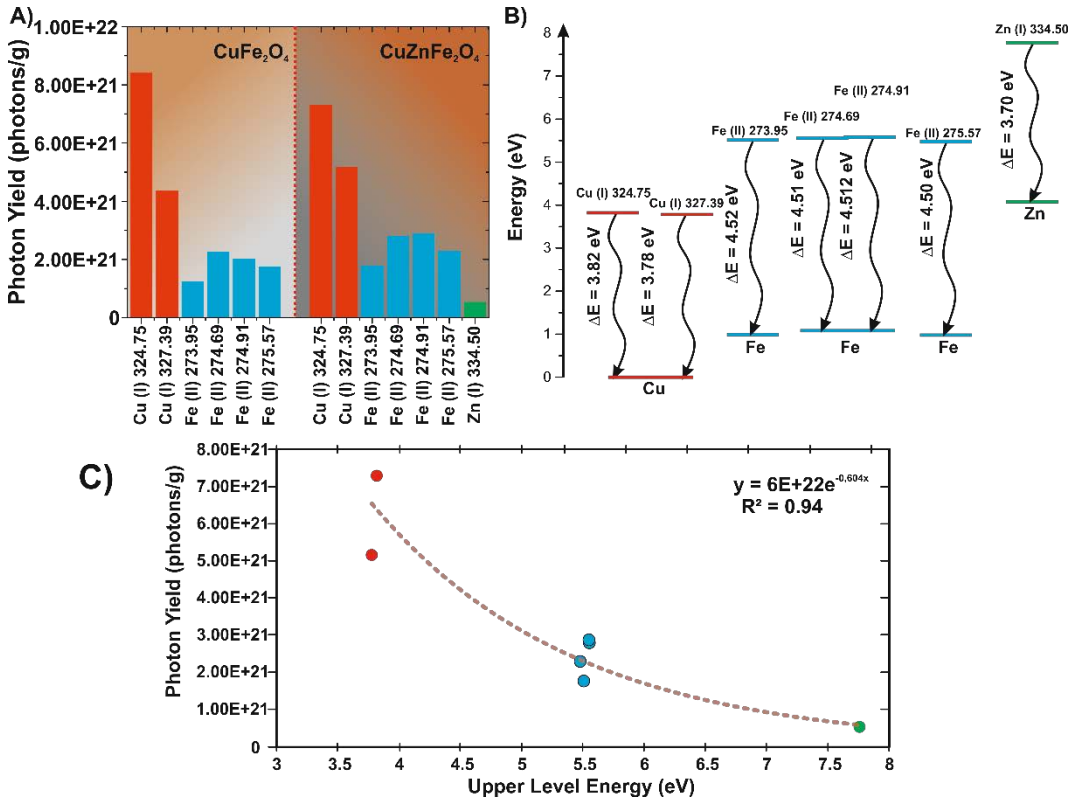

Figure 5. A) Average emission of photons per gram for main lines found in both samples. B) E_1 energies and ΔE of transits in A. C) Exponential fit of photon yield as a function of E_1.

If we consider the finite energy transfer rate in which mechanisms leading to particle atomization and excitation are based, it is reasonable to propose a selective excitation of readily accessible low-lying states in SP-LIBS under the conditions applied herein. E_1 for other observable Fe lines, namely, Fe (II) at 298.31 nm and Fe (I) at 302.04 nm were 5.82 eV and 4.19 eV, respectively. These data are compatible with other transitions. The priority population of low E_1 levels may be of help to anticipate detection feasibility for different elements by OC-OT-LIBS.

Conclusions

Simultaneous multielemental characterization at single particle level using LIBS was demonstrated by probing single 90 nm in diameter NPs of two different oxides, namely $CuFe_2O_4$ and $CuZnFe_2O_4$, with masses in the order of attograms being successfully detected. Limits of detection were set at 575 ag for Fe, 304 ag for Zn and 37 ag for Cu. Quantification of the photon emission by each constituent element revealed similar dissociation and excitation efficiencies for both samples with slight variations arising from the nature of the chemical bonds present in each multi-component matrix. Moreover, an inverse exponential relation was found between photon yield and upper level energy. This correlation complied with mechanisms described in literature for single particle atomization and excitation and provides new insight on the analytical properties of single nanoparticle LIBS studies. An enhanced sampling strategy based in 3D-printed skimmer-like cones was used to double the sampling throughput of OC-OT-LIBS technology for single nanoparticles with respect to the original sampling approach described in previous work. Overall, we expect the results described in this work to impulse OC-OT-LIBS as a tool for efficient panoramic characterization of nanoparticulate materials obviating any previous sample preparation stage and with straightforward data treatment procedures.

AUTHOR INFORMATION

Corresponding Author

* J.J.L.: email, laserna@uma.es; tel, +34951953007

ORCID

Pablo Purohit: 0000-0001-5839-8064

J. Javier Laserna: 0000-0002-2653-9528

Author Contributions

P.P and F.J.F. designed the experiments with input and supervision from J.J.L. P.P. carried out the reported experiments. All authors contributed to data processing and

interpretation.The manuscript was written through contributions of all authors. All authors have given approval to the final version of the manuscript.

Notes

Authors declare no competing financial interest.

ACKNOWLEDGMENTS

Research funded by the Spanish Ministerio de Economia y Com-petitividad under Project CTQ2014-56058P. P. Purohit gratefully acknowledges the concession of a FPI research grant linked to the same project.

References

(1) Markwalter, C. F.; Kantor, A. G.; Moore, C. P.; Richardson, K.A.; Wright, D. W. Chem.Rev. 2019, 119 (2), 1456−1518.
(2) Kukkar, D.; Vellingiri, K.; Kaur, R.; Bhardwaj, S. K.; Deep, A.;Kim, K.-H. Nano Res. 2019, 12 (2), 225−246.
(3) Mottaghitalab, F.; Farokhi, M.; Fatahi, Y.; Atyabi, F.; Dinarvand,R. J. Controlled Release 2019, 295, 250−267.
(4) Moßhammer, M.; Brodersen, K. E.; Kühl, M.; Koren, K.Microchim. Acta 2019, 186 (2), 126.
(5) Aznar, E.; Oroval, M.; Pascual, L.; Murguía, J. R.; Martínez-Mánez, R.; Sancenón, F. Chem. Rev. 2016, 116, 561.
(6) Ariga, K.; Nishikawa, M.; Mori, T.; Takeya, J.; Shrestha, L. K.;Hill, J. P. Sci. Technol. Adv. Mater. 2019, 20 (1), 51−95.
(7) Wang, A.; Yang, H.; Song, T.; Sun, Q.; Liu, H.; Wang, T.; Zeng,H. Nanoscale 2017, 9 (41), 15760−15765.
(8) Oar-Arteta, L.; Aguayo, T.; Remiro, A.; Bilbao, J.; Gayubo, A. G. Ind. Eng. Chem. Res. 2015, 54, 11285−11294.
(9) Li, Y.; Shen, J.; Hu, Y.; Qiu, S.; Min, G.; Song, Z.; Sun, Z.; Li, C. Ind. Eng. Chem. Res. 2015, 54, 9750−9757.
(10) Zhang, T.; Zhu, H.; Croue, J. Environ. Sci. Technol. 2013, 47, 2784−2791.
(11) Cama, C. A.; Pelliccione, C. J.; Brady, A. B.; Li, J.; Stach, E. A.; Wang, J.; Wang, J.; Takeuchi, E. S.; Takeuchi, K. J.; Marschilok, A. C. Phys. Chem. Chem. Phys. 2016, 18, 16930−16940.
(12) Wang, Y.-F.; Sun, L.-D.; Xiao, J.-W.; Feng, W.; Zhou, J.-C.; Shen, J.; Yan, C.-H. Chem. - Eur. J. 2012, 18 (18), 5558−5564.
(13) Zhang, S.; Metin, Ö.; Su, D.; Sun, S. Angew. Chem. 2013, 125 (13), 3769−3772.
(14) Feichtmeier, N. S.; Ruchter, N.; Zimmermann, S.; Sures, B.; Leopold, K. A. Anal. Bioanal. Chem. 2016, 408 (1), 295−305.
(15) Leopold, K.; Brandt, A.; Tarren, H. J. Anal. At. Spectrom. 2017, 32 (4), 723−730.
(16) Dendisová, M.; Jeništová, A.; Parchaňská-Kokaislová, A.; Matějka, P.; Prokopec, V.; Švecová, M. Anal. Chim. Acta 2018, 1031, 1−14.
(17) Feichtmeier, N. S.; Ruchter, N.; Zimmermann, S.; Sures, B.; Leopold, K. A. Anal. Bioanal. Chem. 2016, 408 (1), 295−305.

(18) Montoro Bustos, A. R.; Purushotham, K. P.; Possolo, A.; Farkas, N.; Vladar, A. E.; Murphy, K. E.; Winchester, M. R. Anal. Chem. 2018, 90, 14376−14386.
(19) Gundlach-Graham, A.; Hendriks, L.; Mehrabi, K.; Günther, D. Anal. Chem. 2018, 90 (20), 11847−11855.
(20) Bolea-Fernandez, E.; Leite, D.; Rua-Ibarz, A.; Balcaen, L.; Aramendía, M.; Resano, M.; Vanhaecke, F. J. Anal. At. Spectrom. 2017, 32 (11), 2140−2152.
(21) Laserna, J.; Vadillo, J. M.; Purohit, P. Appl. Spectrosc. 2018, 72, 35−50.
(22) Fortes, F. J.; Moros, J.; Lucena, P.; Cabalín, L. M.; Laserna, J. J. Anal. Chem. 2013, 85, 640−669.
(23) Hahn, D. W.; Omenetto, N. Appl. Spectrosc. 2012, 66, 347−419.
(24) Diwakar, P. K.; Loper, K. H.; Matiaske, A.-M.; Hahn, D. W. J. Anal. At. Spectrom. 2012, 27 (7), 1110.
(25) Järvinen, S. T.; Toivonen, J. Opt. Express 2016, 24 (2), 1314.
(26) Järvinen, S. T.; Saari, S.; Keskinen, J.; Toivonen, J. Spectrochim. Acta, Part B 2014, 99, 9−14.
(27) Fortes, F. J.; Fernández-Bravo, A.; Javier Laserna, J. Spectrochim. Acta, Part B 2014, 100, 78−85.
(28) Purohit, P.; Fortes, F. J.; Laserna, J. J. Spectrochim. Acta, Part B 2017, 130, 75−81.
(29) Purohit, P.; Fortes, F. J.; Laserna, J. J. Angew. Chem., Int. Ed. 2017, 56 (45), 14178−14182.
(30) Hou, J. J.; et al. Opt. Express 2019, 27, 3409.
(31) Hohreiter, V.; Hahn, D. W. Anal. Chem. 2006, 78 (5), 1509−1514.